J. Am. Soc. Mass Spectrom. (2016) 27:233–243
DOI: 10.1007/s13361-015-1290-z

RESEARCH ARTICLE

Characterization of the *Saccharomyces cerevisiae* ATP-Interactome using the iTRAQ-SPROX Technique

M. Ariel Geer, Michael C. Fitzgerald

Department of Chemistry, Duke University, Durham, NC 27708-0346, USA

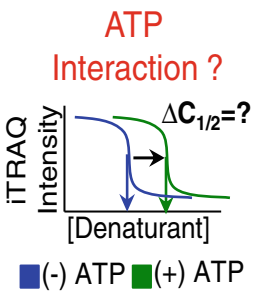

Abstract. The stability of proteins from rates of oxidation (SPROX) technique was used in combination with an isobaric mass tagging strategy to identify adenosine triphosphate (ATP) interacting proteins in the *Saccharomyces cerevisiae* proteome. The SPROX methodology utilized in this work enabled 373 proteins in a yeast cell lysate to be assayed for ATP interactions (both direct and indirect) using the non-hydrolyzable ATP analog, adenylyl imidodiphosphate (AMP-PNP). A total of 28 proteins were identified with AMP-PNP-induced thermodynamic stability changes. These protein hits included 14 proteins that were previously annotated as ATP-binding proteins in the *Saccharomyces* Genome Database (SGD). The 14 non-annotated ATP-binding proteins included nine proteins that were previously found to be ATP-sensitive in an earlier SPROX study using a stable isotope labeling with amino acids in cell culture (SILAC)-based approach. A bioinformatics analysis of the protein hits identified here and in the earlier SILAC-SPROX experiments revealed that many of the previously annotated ATP-binding protein hits were kinases, ligases, and chaperones. In contrast, many of the newly discovered ATP-sensitive proteins were not from these protein classes, but rather were hydrolases, oxidoreductases, and nucleic acid-binding proteins.

Keywords: Mass spectrometry, Proteomics, Thermodynamics, Protein folding, Chemical denaturation, Ligand binding

Received: 19 June 2015/Revised: 1 September 2015/Accepted: 5 October 2015/Published Online: 3 November 2015

Introduction

The interaction of proteins with ligands is a fundamental aspect of protein function, and such interactions are a critical part of many cellular processes including protein activation, cell signaling, and molecular transport. While some protein–ligand binding interactions are well understood, many important biological interactions remain uncharacterized. This is especially true of ubiquitous enzyme cofactor interactions, such as those involving adenosine triphosphate (ATP). ATP is an important cofactor that is required for energy metabolism, protein synthesis, molecular transport across membranes, and protein folding [1–5]. Many proteins interact with ATP to perform their biological functions within the cell. Knowing which proteins are ATP-sensitive (i.e., have direct or indirect interactions with ATP) provides insight into the particular cellular processes in which each protein is involved.

Several different experimental and bioinformatics approaches have been utilized to characterize the ATP-binding properties of proteins. There are currently over 20 X-ray crystallographic structures of *Saccharomyces cerevisiae* proteins that have been solved with ATP [6–25]. A significantly larger number of *Saccharomyces cerevisiae* proteins have been predicted to bind ATP using bioinformatics approaches. For example, a gene ontology (GO)-term analysis of ATP-binding proteins in the *Saccharomyces* Genome Database (SGD) identifies 668 ATP-binding proteins. More recently, mass spectrometry-based proteomics techniques have been exploited for large-scale analyses of ATP-sensitive proteins [26–36]. Such large-scale analyses have involved the use of chemical probes or different energetics-based methods to identify ATP-sensitive proteins on the proteomic scale. Chemical probes such as acyl phosphates that interact with lysine residues in ATP binding sites of proteins have been used to identify human protein kinases and to evaluate novel kinase inhibitors [26–30]. Isotope-coded ATP probes (ICAPs) have also been used in several studies to discover novel ATP-binding motifs [31, 32].

Electronic supplementary material The online version of this article (doi:10.1007/s13361-015-1290-z) contains supplementary material, which is available to authorized users.

Correspondence to: Michael Fitzgerald;
e-mail: michael.c.fitzgerald@duke.edu

The Cellular Thermal Shift Assay (CETSA) and several energetics-based approaches, including the pulse proteolysis and stability of proteins from rates of oxidation (SPROX) techniques, have also been used for the large-scale analysis of the ATP interactome in different organisms (e.g., *Escherichia coli* and *Saccharomyces cerevisiae* [33–35]) and in a cancer cell line (e.g., the K562 chronic myeloid leukemia cell line) [36].

A significant issue with all the mass spectrometry-based approaches, reported to date, for the large-scale analysis of ATP interacting proteins is their ability to provide a comprehensive analysis of all the proteins in a proteome that are ATP-sensitive. In some experimental approaches (e.g., in SPROX) the number of proteins that are effectively assayed for ATP interactions is known (i.e., both "hit" and "non-hit" proteins are specifically identified). For example, the SILAC-SPROX approach recently employed for the large-scale analysis of ATP-interacting proteins in the *Saccharomyces cerevisiae* proteome enabled the analysis of 526 yeast proteins for ATP interactions and resulted in the identification of 139 ATP-sensitive proteins [35]. In other approaches (e.g., in experiments using chemical probes) the number of proteins effectively assayed is less clear because the read-out only involves the detection and identification of protein hits. Another significant challenge associated with the above mass spectrometry-based proteomics approaches for the identification of ATP-sensitive proteins is the separation of true positives from false positives.

As part of this work, novel ATP interacting proteins in the *Saccharomyces cerevisiae* proteome were discovered using SPROX with an isobaric mass tagging strategy (iTRAQ-SPROX). The iTRAQ-SPROX methodology is related to the SILAC-SPROX methodology that was previously used to study the ATP interactome in *Saccharomyces cerevisiae* [35]. The iTRAQ- and SILAC-SPROX techniques both report on the same chemical denaturant-dependent unfolding properties of proteins and protein–ligand complexes. However, because of their use of different quantitative proteomics strategies, the proteomic coverage achieved in each method is different, with only a fraction of the assayed proteins in each technique overlapping. One goal of this work was to increase the proteomic coverage of the SPROX experiments to identify ATP-sensitive proteins in the *Saccharomyces cerevisiae* proteome. A second goal of this work was to evaluate both the complementarity and consistency of the iTRAQ- and SILAC-SPROX methodologies.

Experimental

Materials

A non-hydrolysable ATP mimic, adenyl imidodiphosphate (AMP-PNP), was purchased from Calbiochem (San Diego, CA, USA). Tris (2-carboxyethyl)phosphine hydrochloride (TCEP) was purchased from Thermo Fisher Scientific (Waltham, MA, USA). The *Saccharomyces cerevisiae* strain used in this work (Y258) was purchased from Open Biosystems. All other chemicals were purchased from Sigma-Aldrich (St. Louis, MO, USA).

iTRAQ-SPROX Protocol

The two iTRAQ-SPROX experiments described here were performed using the iTRAQ-SPROX protocol described in reference [37]. In Experiment 1, a yeast lysate containing 8 μg/μL of total protein prepared in 0.1 M Tris-HCl buffer, pH 7.4, was divided into two 144 μL portions, and 18 μL of 1 M $MgCl_2$ was added to each portion. The (–) Control sample was created by adding 18 μL of H_2O to one portion of the lysate. The (+) AMP-PNP sample was created by adding 18 μL of an 823 mM stock solution of AMP-PNP prepared in H_2O to the second portion. Both (–) and (+) samples were equilibrated for 1 h on ice before 20 μL of each equilibrated sample was diluted into 75 μL of urea buffers containing 0.1 M Tris-HCl (pH 7.4) and the following urea concentrations: 0, 1.3, 2.6, 3.7, 4.5, 5.3, 6.4, and 8 M. The final urea concentrations in each buffer were 0, 1.0, 2.0, 2.7, 3.4, 4.0, 4.8, and 6.0 M. The total amount of protein in each buffer was 128 μg, and the final concentration of AMP-PNP was 16 mM. The samples in the urea-containing buffers were equilibrated for 1 h at room temperature before the methionine oxidation reaction was initiated with the addition of 5 μL of H_2O_2. The oxidation reactions in the urea-containing buffers were allowed to proceed for 6 min before they were quenched with 1 mL of 300 mM methionine.

The proteins in each sample were precipitated by the addition of 160 μL of 100% trichloroacetic acid (TCA) (wt/vol) and incubated on ice at 4°C overnight. The samples were centrifuged at 8000 rcf for 30 min at 4°C and the supernatant was decanted. The protein pellets were washed three times with 300 μL of ice-cold ethanol. The ethanol was decanted, and the protein pellets were dried in a fume hood. The protein pellets were dissolved in 30 μL of 0.5 M triethylammonium bicarbonate (TEAB) with 0.1% final concentration of SDS. The samples were vortexed, heated at 60°C, and sonicated for 10 min at a time for 2–3 cycles. The disulfide bonds were reduced with a final concentration of 5 mM tris(2-carboxyethyl)phospine (TCEP) for 1 h at 60°C. The free cysteine residues were alkylated with a final concentration of 10 mM methyl methanethiosulfonate (MMTS) for 10 min at room temperature. The proteins were digested with 1.5 μL of 1 mg/mL trypsin at 37°C for 16 h.

The 0, 1.0, 2.0, 2.7, 3.4, 4.0, 4.8, and 6.0 M (–) and (+) AMP-PNP samples were labeled with the 113, 114, 115, 116, 117, 118, 119, and 121 iTRAQ reagents from an iTRAQ 8-plex AB Sciex, Pte, Ltd, (Framingham, MA, USA) according to the manufacturer's protocol, with the exception that 0.5 unit instead of 1 unit of each reagent was used. A 40-μL aliquot of each sample was combined within a set, (–) or (+), and 80 μL of each combined sample was removed to create the non-enriched samples. The remaining combined samples were placed on a Speed Vac concentrator to reduce the sample volume to ~50 μL. The samples were then enriched for methionine-containing peptides using a Pi^3 - Methionine Reagent kit The Nest Group (Southborough, MA, USA) according to the manufacturer's

protocol. The non-enriched and methionine-enriched samples were both diluted in 0.1% or 2% TFA, respectively, and further desalted using C18 resin (The Nest Group). The C18 resin was wetted with 400 µL of methanol and rinsed with 400 µL of 2% TFA. Each sample was loaded in two batches, the resin was rinsed twice with 2% TFA, and peptides were eluted with 50 µL of 30% acetonitrile/0.1% TFA, then twice with 50 µL of 70% acetonitrile/0.1% TFA.. Samples were placed on a Speed Vac concentrator to remove acetonitrile and the sample volume was reduced to ~50 µL. The samples were diluted with 0.1% TFA prior to LC-MS/MS analysis.

In Experiment 2, the yeast lysate concentration was ~9 mg/mL. The initial urea concentrations in 0.1 M Tris-HCl buffers, pH 7.4 were 0, 2.0, 2.6, 3.3, 3.6, 4.4, 5.3, and 6.4 M. The final urea concentrations in 0.1 M Tris-HCl buffer (pH 7.4) during the methionine oxidation reaction were 0, 1.5, 2.0, 2.4, 2.7, 3.4, 4.0, and 4.8 M. The oxidation reactions were allowed to proceed for 24 min. The 0, 1.5, 2.0, 2.4, 2.7, 3.4, 4.0, and 4.8 M urea samples were labeled with 0.5 unit of the 113, 114, 115, 116, 117, 118, 119, and 121 iTRAQ tags, respectively. The (–) Control and (+) AMP-PNP samples were not enriched for methionine residues.

LC-MS/MS Analyses

LC-MS/MS analyses for ATP Experiment 1 were performed on an Orbitrap Elite ETD mass spectrometer equipped with an Easy-nLC 1000 system. The trapping column was a 100 µm × 2 cm Integrafrit column New Objective (Woburn, MA, USA) packed with 200 Å Magic C18 AQ 5 µm material Bruker-Micrhom, Inc. (Auburn, CA, USA). The column was a 75 µm × 25 cm PicoFrit column (New Objective) packed with 100 Å Magic C18 AQ 5 µm material (Michrom). The flow rate was set to 400 nL/min. Solvent A consisted of 0.1% formic acid in H_2O and solvent B was 0.1% formic acid in acetonitrile. The LC gradient increased from 5% to 7% B over 2 min, 7% to 35% B over 90 min, 35% to 50% B over 1 min, was isocratic at 50% B for 9 min, increased from 50% to 95% B over 1 min, and finally isocratic at 95% B for 8 min. Product ion scans (resolution 15,000) were collected for the 10 ions with the most intense peaks in a given precursor scan (resolution 60,000) with an intensity threshold of 5000. The dynamic exclusion window of a given *m/z* ratio was set at 1 scan in 0.75 min and the precursor isolation width was 1.2 *m/z*. The scan range for the precursor scan was 400–1800 *m/z* and 100–2000 *m/z* for the product ion scan. Collision induced dissociation was achieved using higher-energy collisional induced dissociation (HCD) with a normalized collision energy of 40% and an HCD activation time of 0.1 ms.

LC-MS/MS analyses for Experiment 2 were performed on a Thermo Scientific Q-Exactive Plus high-resolution mass spectrometer with a nanoAcquity UPLC system Waters Corporation, (Milford, MA, USA) and a nanoelectrospray ionization source. Approximately 2 µL containing an estimated 0.1 µg of each sample was injected and trapped on a Symmetry C18 300 mm × 180 µm trapping column for 3 min at 5 µL/min (99.9/0.1 v/v water/acetonitrile 0.1% formic acid), followed by the analytical separation on a 75 µm × 250 mm column packed with 1.7 µm Acquity HSST3 C18 stationary phase (Waters Corp). Peptides were separated using a gradient of 3% to 30% acetonitrile with 0.1% formic acid over 90 min at a flow rate of 0.4 µL/min with a column temperature of 55°C. Data collection on the Q-Exactive Plus mass spectrometer was performed in a data-dependent acquisition (DDA) mode with a resolution of 70,000 (at a *m/z* 200) for full MS scan from *m/z* 375 – 1600 with a target AGC value of 1 x 10^6 ions in profile mode, followed by 20 MS/MS scans with a resolution of 17,500 at a *m/z* 200 in centroid mode, using an AGC target value of 1×10^5 ions, a max fill time of 60 ms, and normalized collision energy of 30 V. A 30 s dynamic exclusion was employed to decrease MS/MS oversampling.

The LC-MS/MS data from Experiment 1 acquired on the Orbitrap Elite were searched against the SwissProt *Saccharomyces cerevisiae* database using Proteome Discoverer. Search parameters included fixed modification of MMTS on cysteine residues, fixed modification of iTRAQ 8-Plex on N-terminus and lysine residues, a variable modification of oxidation on methionine residues, and two missed cleavage sites were allowed. The precursor mass tolerance was set to 10 ppm and the fragment mass tolerance was set to 0.8 Da. The LC-MS/MS data from ATP Experiment 2 acquired on the Q-Exactive Plus were searched against the SwissProt *Saccharomyces cerevisiae* database using Spectrum Mill. Search parameters were the same as previously stated, except that the precursor mass tolerance was set to 10 ppm and the fragment mass tolerance was set to 20 ppm. In both Experiment 1 and Experiment 2, peptides identified with a false discovery rate (FDR) of <5% were used for data analysis.

iTRAQ-SPROX Data Analysis

The SPROX data were analyzed as previously described [37]. Briefly, the identified peptide sequences and their iTRAQ reporter ion intensities were exported into Excel along with the filename, identification, score, charge state, modifications, isolation purity, retention time, protein accession number, and protein name. Only peptides with high quality quantitative data (i.e., iTRAQ reporter ion intensities at *m/z* 113–121 that summed to >1000) were used in analyses. The iTRAQ reporter ion intensities for an individual peptide were normalized as we have previously described [37]. The normalized iTRAQ reporter ion intensities were used to generate chemical denaturation data sets for the peptides successfully quantified in each of the SPROX experiments.

In each experiment, a set of peptides with normalized iTRAQ reporter ion differences that resulted in significant transition midpoint shifts were identified by a visual inspection of the data after a difference analysis, as described in the Supporting Information. Significant transition midpoint shifts were taken to be those resulting from iTRAQ reporter ion differences in the (–) and (+) AMP-PNP samples at two or more consecutive iTRAQ tags, where at least one difference was between the transition regions of the two chemical

denaturation curves obtained with and without ligand. Significant iTRAQ reporter ion differences were taken to be <–0.15 and >0.17, based on a global analysis of the data, in which these values represented the 22nd and 78th percentiles of the iTRAQ reporter ion difference distribution (see Supplementary Figure S1). This requirement for hits to have two consecutive iTRAQ reporter ion differences less than the 22nd percentile or greater than the 78th percentile produced hit peptides with an estimated *P*-value <0.05. More detailed information on hit selection is provided in the Supporting Information.

Quantitation of Protein-ATP Binding

The transition midpoint shifts of the hit peptides were used to generate $\Delta C_{1/2}$ values, which are defined as the transition midpoint difference between the (–) Control and (+) AMP-PNP samples. The $\Delta C_{1/2}$ value was then used to calculate a binding free energy ($\Delta\Delta G$) for the protein–ligand binding interaction using Equation 1.

$$\Delta\Delta G = -m \times \Delta C_{1/2} \quad (1)$$

In Equation 1, $\Delta\Delta G$ is the binding free energy, m is $\delta\Delta G/\delta\Delta C_{1/2}$, and $\Delta C_{1/2}$ is the difference in the transition midpoints between the (–) Control and (+) AMP-PNP data sets, where a positive value represents an increased urea concentration in the presence of ligand. A m-value of 1.3 kcal mol^{-1} M^{-1} for urea was used for all proteins. This m-value was estimated based upon the average protein domain size of 100 amino acids and the average contribution of 0.013 kcal mol^{-1} M^{-1} of urea per amino acid to the m-value of the protein as determined in reference [38]. Equation 2 was then used to calculate the dissociation constant (K_d) for the protein–ligand interaction.

$$K_d = [L] / \left(e^{-\Delta\Delta G / nRT} - 1 \right) \quad (2)$$

In Equation 2, [L] is the concentration of free ligand, n is the number of independent binding sites, R is the universal gas constant, and T is the temperature in Kelvin. Since the concentration of AMP-PNP was in large excess over the concentration of any individual protein in the lysate, the [L] was taken to be the final concentration of AMP-PNP in the reaction buffers, which was 16 mM in each experiment. For these calculations, n was assumed to be 1, R was 0.001987 kcal mol^{-1} K^{-1}, and T was 298 K.

Bioinformatics Analyses

Protein interaction networks were generated using the STRING database [39]. The interaction networks were constructed using the active prediction methods in STRING based only on experiments, and only interactions with high confidence levels were included. Known ATP-binding proteins were identified using the *Saccharomyces* Genome Database (SGD) and the Gene Ontology term, "ATP Binding" (code 0005524).

Results

Discovery of ATP-Interacting Proteins

The non-hydrolyzable ATP mimic, AMP-PNP (Figure 1), was used in two iTRAQ-SPROX experiments to identify ATP-interacting proteins in yeast cell lysates. The experimental workflow in each experiment (see Figure 2) was the same as were the experimental conditions with the exception of the hydrogen peroxide reaction time employed in the iTRAQ-SPROX protocol, which was 6 and 24 min in Experiments 1 and 2, respectively. In theory, the hydrogen peroxide reaction time should not impact detection of protein–ligand binding hits in iTRAQ-SPROX experiments, as long as the time is sufficient to ensure that the oxidation reaction of an unprotected methionine residue proceeds to completion (>3 half-lives) and short enough to preclude quantitative oxidation of globally protected methionine residues [40]. This former condition was true for both reaction times, and the latter condition was assumed to be true for the assayed proteins. In Experiment 1, a methionine-containing peptide enrichment was performed to increase the coverage of methionine-containing peptides. A methionine peptide enrichment step was not performed in Experiment 2. We reasoned that the fraction of unmodified methionine-containing peptides (i.e., those amenable to enrichment) in Experiment 2 was small because of the long H_2O_2 exposure. Therefore, the enrichment step was not deemed cost-effective.

The proteomic coverage obtained in each iTRAQ-SPROX experiment is summarized in Table 1. The number of peptides and proteins assayed in Experiment 1 was higher than that in Experiment 2 because of the use of the methionine-containing peptide enrichment strategy employed in Experiment 1. A total of 373 unique proteins were assayed for AMP-PNP interactions in the two experiments. These assayed proteins included those with methionine-containing peptide probes that were successfully detected and quantified in the bottom-up shotgun proteomics analyses of both the plus and minus ligand samples from each experiment. Summarized in Supplementary Table S1 are the iTRAQ-SPROX data sets generated for each protein assayed in the (+) and (–) AMP-PNP samples.

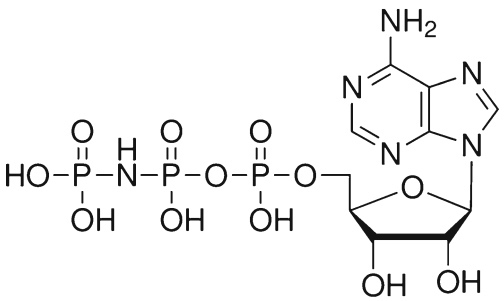

Figure 1. Chemical structure of AMP-PNP, the non-hydrolyzable ATP mimic used in this ATP-binding study

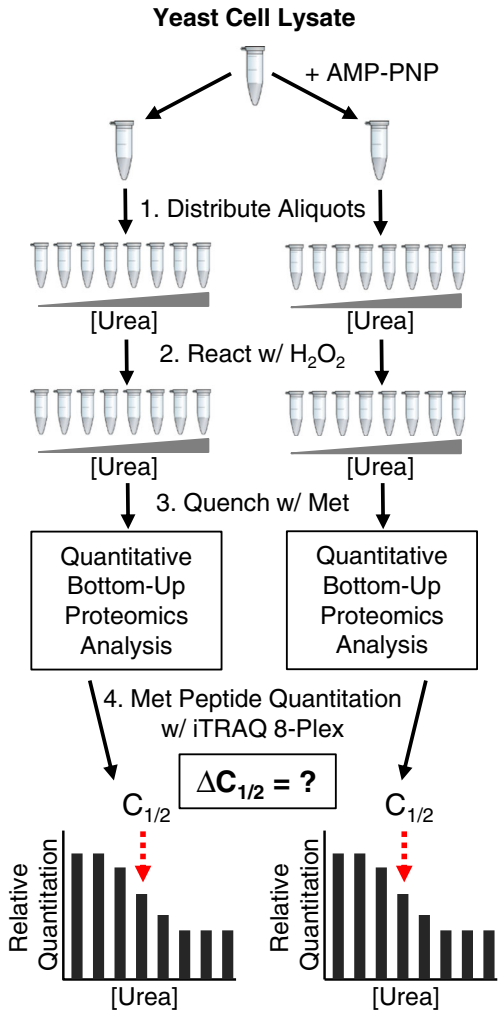

Figure 2. Schematic representation of the experimental workflow used in this study

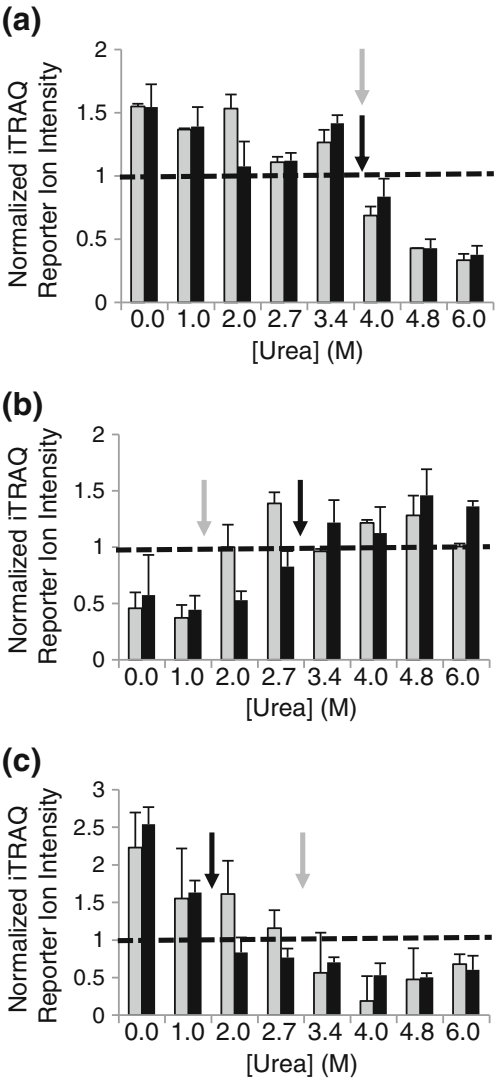

Figure 3. Representative iTRAQ-SPROX data obtained in ATP-binding experiments. (**a**) Chemical denaturation data recorded in Experiment 1 for an unmodified methionine-containing peptide (GKGVQELMAK) from the non-hit protein, fumarate reductase. (**b**) Chemical denaturation data recorded in Experiment 1 for an oxidized methionine-containing peptide (TVM(ox)IAAHGNSLR) showing an ATP-induced stabilization for the hit protein, phosphoglycerate mutase 1. (**c**) Chemical denaturation data recorded in Experiment 1 for an unmodified methionine-containing peptide (LIDLTQFPAFVTPMGK) showing an ATP-induced destabilization for the hit protein, pyruvate decarboxylase. The light and dark shaded bars represent the data collected in the absence and in the presence of the ATP ligand, respectively. The averaged data extracted from the multiple product ion mass spectra generated in the shotgun proteomics analyses performed in each experiment are shown with the error bars representing ±1 SD. The dotted line indicates the normalized reporter ion intensity that separates the pre- and post-transition baselines. The arrows point to the denaturant concentration at the $C_{1/2}$ value extracted from each data set

Shown in Figure 3 are iTRAQ-SPROX data sets for methionine-containing peptide probes showing hit and non-hit behavior. An iTRAQ-SPROX data set for a methionine-containing peptide probe from fumarate reductase, a non-hit protein, is shown in Figure 3a. Shown in Figure 3b is an iTRAQ-SPROX data set for a methionine-containing peptide hit from phosphoglycerate mutase (P00950), which was previously identified as an ATP-sensitive protein in SILAC-SPROX experiments [35]. This methionine-containing peptide probe from phosphoglycerate mutase showed hit behavior in both Experiments 1 and 2 with ATP-induced stabilizations in each experiment. The stabilizations (i.e., $\Delta C_{1/2}$ values of 1.0 and 1.1 M) were used to calculate K_d values for the protein-ATP binding interaction of 2.0 and 1.6 mM in Experiments 1 and

Table 1. Summary of Proteomics Results. Total Assayed Peptides are Those That Contain the Same Methionine-Containing Peptide Sequence but May be Either Unmodified or Oxidized

Experiment	Oxidation time (min)	Assayed peptides	Assayed proteins	Hit peptides (proteins)
1	6	777	372	25 (22)
2	24	92	67	8 (7)
Total	-	845	373	33 (28)

2, respectively. Unfortunately, the data analysis methods used in this work preclude the inclusion of error bars for the $\Delta C_{1/2}$ and K_d values determined here. However, the replicate data generated for the TVMIAAHGNSLR peptide from phosphoglycerate mutase (see Table 2) provide a measure of the precision with which $\Delta C_{1/2}$ and K_d values can be determined in iTRAQ-SPROX.

Shown in Figure 3c is an iTRAQ-SPROX data set from Experiment 1 for pyruvate decarboxylase (P06169), which was detected as a hit in both iTRAQ-SPROX experiments, albeit with different peptide probes in each experiment. The chemical denaturation behaviors observed for two of the three methionine-containing peptides from pyruvate decarboxylase are consistent with ligand-induced destabilizations, and the chemical denaturation data generated for the third peptide were consistent with a destabilization. Pyruvate decarboxylase was also detected as a hit protein in the SILAC-SPROX experiments [35]. Neither phosphoglycerate mutase nor pyruvate decarboxylase is annotated in the SGD with the GO-term "ATP-binding."

In total, 28 unique proteins with 33 peptide probes were detected as ATP-interacting hits in the two iTRAQ-SPROX experiments described here (see Table 2). The 33 peptide hits have an estimated *P*-value <0.05 (see iTRAQ-SPROX Data Analysis in Experimental Procedures). Of these 28 proteins, two proteins were consistently identified as ATP-interacting protein hits in both experiments (see Table 2), whereas 18 of the remaining 26 protein hits were only assayed in one experiment. In order to be included in the assay, the same methionine-containing peptide probe from a protein had to be successfully identified and quantified in both the (+) and (–) AMP-PNP samples. A total of eight protein hits (five from Experiment 1 and three from Experiment 2) were identified as a hit in one experiment and not in the other (see Table 2).

Approximately half of the ATP-sensitive protein hits identified here were previously annotated in the SGD as ATP-binding proteins (see Table 2). This fraction is slightly larger than that found in the SILAC-SPROX experiments, where only one-third of the protein hits identified were previously annotated as ATP-binding proteins [35]. A total of 92 of the 373 unique proteins assayed in these iTRAQ-SPROX experiments are annotated as "ATP-binding" in the SGD. Only 14 of these 92 proteins were identified as hits in the AMP-PNP binding experiments described here. A larger fraction of the annotated ATP-binding proteins (37 out of 109) were detected as hits in the SILAC-SPROX experiment. The decreased sensitivity of iTRAQ-SPROX to previously annotated hits may be due to the decreased number of data points (eight instead of the 10) used in SILAC-SPROX to define the chemical denaturation behavior.

ATP-Induced Stabilization Versus Destabilization

The direction (e.g., stabilizing or destabilizing) and magnitude of the observed $\Delta C_{1/2}$ value shifts of all the hit peptides detected in the iTRAQ-SPROX experiments performed here are shown in Table 2. Approximately half of the hits resulted from ATP-induced stabilizations. Direct ATP binding to the native state of a protein is expected to increase the stability of the protein (or protein folding domain to which ATP binds). The magnitude of a ligand-induced stabilization resulting from such direct protein-ATP binding interaction can be measured in the iTRAQ-SPROX experiment (see Figure 3b) and used in Equations 1 and 2 to calculate K_d values. A total of 13 AMP-PNP-induced stabilizations were detected in this work (Table 2). The K_d values calculated from these ligand-induced stabilizations ranged from <100 μM to 2.0 mM, which is in the range of previously reported ATP binding affinities [41–43].

Close to half of the observed $C_{1/2}$ value shifts indicated a decrease in protein stability in the presence of AMP-PNP (Table 2). Such ligand-induced destabilizations can result from several different phenomena. AMP-PNP binding to one region of a protein could induce conformational changes that are destabilizing in another region of the protein [44]. Alternatively, because the iTRAQ-SPROX experiment is performed in the context of all of the proteins in a cell lysate, AMP-PNP binding to one protein could induce conformational changes that are destabilizing to another protein. Cases in which AMP-PNP interacts with non-native states of the protein could also result in an apparent destabilization. This latter phenomenon was observed for glyceraldehyde 3-phosphate dehydrogenase (GAPDH) in an ATP-binding study performed using the proteins in an *Escherichia coli* cell lysate using pulse proteolysis [33, 43]. A similar destabilization of *Saccharomyces cerevisiae* GAPDH was also observed in SILAC-SPROX [35].

GAPDH was not detected as a hit in the iTRAQ-SPROX experiments reported here, even though it was assayed with three methionine-containing peptide probes, two of which overlapped with those detected as hits in the SILAC-SPROX experiment. One of the overlapping peptides (PMFVMGVNEEK) showed a destabilization in the iTRAQ-SPROX experiment (Supplementary Table S1). However, the peptide did not meet our hit criteria (because the transition midpoint shift was too small (i.e., <1 M) and not deemed statistically significant (see iTRAQ-SPROX Data Analysis section in Experimental). The use of only eight denaturant concentrations in iTRAQ-SPROX (as opposed to 10 in SILAC-SPROX) can limit the sensitivity of iTRAQ-SPROX. This may also explain why the overall peptide hit rate in iTRAQ-SPROX (~8%) was lower than that observed in SILAC-SPROX (~26%).

ATP binding can produce both stabilizing and destabilizing effects in the same protein. Such a scenario was observed in the case of pyruvate decarboxylase. Such ligand-induced stabilizations and destabilizations could arise from allosteric effects in which ligand binding to one region of the protein may induce conformational changes in another region of the protein. The destabilizations detected for pyruvate decarboxylase and other proteins hits in this study could also result from AMP-PNP binding events that disrupt protein–protein interactions. For

Table 2. Summary of Peptide and Protein Hits Identified in the Two ATP Binding Experiments Performed Using iTRAQ-SPROX

Accession number, protein name, and peptide sequence	Experiment	$\Delta C_{1/2}$ (M)	K_d (mM)
(P00549) Pyruvate kinase, CDC19[a,b]	1	–2.2	-
IMYVDK			
(P00950) Phosphoglycerate mutase, GPM1[b]	1	1.0	2.0
TVM(ox)IAAHGNSLR	2	1.1	1.6
TVMIAAHGNSLR			
(P02994) Elongation factor 1 alpha, TEF1[b]	2	–2.0	-
SVEM(ox)HHEQLEQGVPGDNVGFNVK			
(P04046) Phosphoribosylpyrophosphate amidotransferase, ADE4	1	1.4	0.7
EIVNMAK	1	1.3	0.9
VSGLAGSMGIAHLR			
(P04801) Threonyl-tRNA synthetase, THS1[a,d]	2[c]	>2.2	<0.1
EATSWETTPM(ox)DIAK			
(P04807) Hexokinase isoenzyme 2, HXK2[a,b]	1	–1.0	-
FDKPFVMDTSYPAR			
(P05030) Plasma membrane P2-type H+-ATPase, PMA1[a]	1	–1.5	-
RGEGFMVVTATGDNTFVGR			
(P06169) Pyruvate decarboxylase, PDC1[b]	1	–1.5	-
LIDLTQFPAFVTPMGK	1	+1.5	-
LLQTPIDMSLKPNDAESEK	2[c]	–1.3	-
NATFPGVQM(ox)K			
(P07263) Histidine tRNA synthetase, HTS1[a,b]	1	–1.0	-
QGLDDIATLMK			
(P08566) Pentafunctional arom protein, ARO1[a]	1	–1.2	-
MQQRPIAPLVDSLR			
(P0CX41) Ribosomal 60S subunit protein L23A, RPL23A[b]	1[c]	–1.7	-
VM(ox)PAIVVR			
(P0CX55) Protein component of the small (40S) ribosomal subunit, RPS18A[b]	1	1.0	2.0
IVQIM(ox)QNPTHYK			
(P10081) Translation initiation factor eIF4A, TIF1[a,b]	2[c]	1.4	0.7
FDDM(ox)ELDENLLR			
(P10591) Heat shock protein 70 family protein, SSA1[a,b]	1	–2.2	-
ELQDIANPIMSK			
(P10592) Heat shock protein 70 family protein, SSA2[a,b]	2[c]	<–1.8	-
NQAAM(ox)NPANTVFDAK			
(P14126) Ribosomal 60S subunit protein L3, RPL3[b]	2	1.3	0.9
AGM(ox)TTIVR			
(P15180) Lysyl-tRNA synthetase, KRS1[a,b]	1	–1.3	-
RINMIEELEK			
(P16521) Translation elongation factor 3, YEF3[a,b]	1[c]	>2.0	<0.2
QINENDAEAMNK			
(P17255) Subunit A of the V1 membrane domain of VATPase, VMA1[a,d]	1[c]	1.2	1.1
TTLVANTSNMPVAAR			
(P17709) Glucokinase, GLK1[a,d]	1	–1.0	-
RTLAFMK			
(P19097) Alpha subunit of fatty acid synthetase, FAS2[b]	1	<–2.7	-
VVEIGPSPTLAGM(ox)AQR			
(P25491) Type I HSP40 co-chaperone, YDJ1[a,d]	1[c]	1.0	2.0
VGIVPGEVIAPGMR			
(P32324) Elongation factor 2, EFT2[b]	2[c]	–0.7	-
STAISLYSEMSDEDVK	2	1.1	1.6
STAISLYSEM(Ox)SDEDVK			
(P39522) Dihydroxyacid dehydratase, ILV3[b]	1	–1.0	-
TMELGILPR			
(P41805) Ribosomal 60S subunit protein L10, RPL10	1	–2.5	-
LQQGMR			
(P53090) Aromatic aminotransferase I, ARO8	1	–1.0	-
MDSFSK			
(Q06252) Protein with similarity to Tfs1p, YLR179C	1	1.0	2.0
SQLSAEDKLALLMTDPDAPSRTEHK			
(Q12377) Non-ATPase subunit of the 26S proteasome lid, RPN6	1	<–2.4	-
ELM(ox)GDELTR			

[a]Annotated with the GO Term "ATP-binding" in the *Saccharomyces* Genome Database
[b]Protein was also identified as an ATP-binding protein in SILAC-SPROX experiments described in reference [35]
[c] Peptide displayed inconsistent iTRAQ-SPROX behavior in the two experiments (i.e., it was assayed in both experiments but only identified as a hit in one experiment)
[d]Protein was not identified as an ATP-binding protein in SILAC-SPROX experiments described in reference [35], even though the same methionine-containing peptide probe was assayed

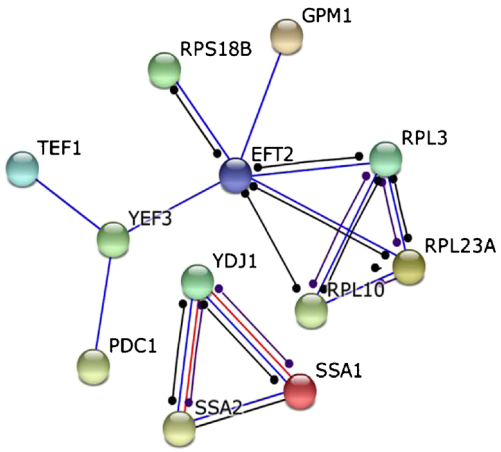

Figure 4. Schematic representation of the protein interaction network generated using the STRING database to analyze the 28 ATP-sensitive protein hits identified in this work. Shown are the 14 protein hits that were found to interact with at least one or more of the other identified protein hits. The lines connecting the proteins, which are represented by the filled circles, indicate protein–protein interactions that are known based on experimental data. Blue lines indicate direct binding interactions. Other direct physical and functional interactions such as inhibition, catalysis, and reaction are indicated by red, purple, and black lines, respectively. White lines indicate indirect physical and functional interactions (e.g., connections made using the results of tandem affinity purification experiments)

example, a direct AMP-PNP binding interaction with one protein may cause another protein to be destabilized due to the disruption of a protein-protein interaction. Analysis of the 28 AMP-PNP-sensitive protein hits detected in the iTRAQ-SPROX experiments described here using the STRING database [39] revealed that 14 of the 28 protein hits are known to directly interact with at least one or more of the other identified protein hits (Figure 4).

The STRING database analysis (Figure 4) can also be used to speculate about the networks of protein–protein interactions that are involved in the ATP-interactome. For example, three of the AMP-PNP interacting hits identified here [including translation elongation factor 3 (YEF3), elongation factor 1α (TEF), and pyruvate decarboxylase (PDC1)] are involved in a known protein interaction network (see Figure 4). One protein in the network, YEF3, is a previously annotated ATP-binding protein that was found to be stabilized in the presence of AMP-PNP in the iTRAQ-SPROX experiments described here. The other two proteins in the network, TEF1 and PDC1, were non-annotated ATP-binding proteins, which were each found to be destabilized in the presence of AMP-PNP. One hypothesis is that the direct binding of ATP to YEF3 may disrupt protein–protein interactions involving the two non-annotated ATP-binding proteins, TEF1 and PDC1. Additional ATP-binding experiments utilizing the purified proteins and defined mixtures containing these proteins using SPROX or other experimental approaches are needed to evaluate the above hypothesis.

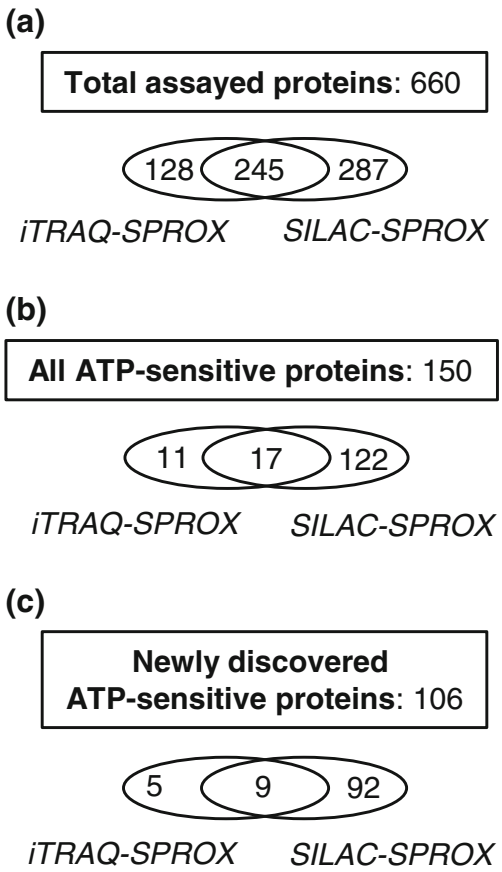

Figure 5. Venn diagram showing overlap between the iTRAQ-SPROX data generated in this work and the SILAC-SPROX data generated in reference [35]

Overlap with SILAC-SPROX

A goal of this work was to compare the proteomic coverage and the ATP-sensitive hits in this work to the results previously reported in SILAC-SPROX experiments [35]. The experimental overlap between the two experiments is summarized in Figure 5. A total of 245 proteins were assayed in both the iTRAQ-SPROX experiments described here and the SILAC-SPROX experiments reported previously (Figure 5a). The 245 overlapping proteins included a total of 17 overlapping protein hits (see Figure 5b and Table 2). A total of 9 of these overlapping protein hits are newly discovered ATP-sensitive proteins that are not annotated as "ATP-binding" in the SGD (Figure 5c).

The SILAC-SPROX approach enables the use of two different proteomics readouts (one involving a solution-based strategy and one involving a gel-based strategy) [35]. As expected, most (i.e., 13 out of 17) of the overlapping hits in the iTRAQ-SPROX and SILAC-SPROX experiments were those that were identified in the solution-phase SILAC-SPROX experiments [35]. Such a large degree of overlap between iTRAQ-SPROX and solution-phase SILAC-SPROX data is expected because both approaches rely on the detection and quantitation of peptide probes containing the same methionine residue. It is also noteworthy that the ATP-induced

stabilizations and destabilizations detected in iTRAQ-SPROX were consistent with those determined in the solution phase SILAC-SPROX experiment, with only two exceptions [Ribosomal protein S18 (P0CX55) and elongation factor 2 (EFT2)].

Three of the overlapping protein hits (i.e., TEF, PDC1, and YEF3) in the iTRAQ- and SILAC-SPROX experiments were previously detected as hits only in the gel-based SILAC-SPROX experiments [35]. The gel-based readout in SILAC-SPROX is advantageous because it enables every peptide that is successfully identified and quantified in the shotgun proteomics analysis (methionine-containing or not) to report on the ligand binding properties of the protein from which it was derived. However, the gel-based SILAC-SPROX experiment has the drawback that it only yields protein-level information and that the direction of the protein stability change (e.g., stabilization or destabilization) cannot always be ascertained from the data [35]. This is in contrast to iTRAQ-SPROX and the solution-phase SILAC-SPROX experiment, which directly reports on the stabilization or destabilization of the protein domain from which the detected peptide probe was derived. The newly collected iTRAQ-SPROX data reveal that the domains assayed for elongation factor 1 A are destabilized in the presence of AMP-PNP, while elongation factor 3 was stabilized in the presence of ATP (see Table 2). In the case of pyruvate decarboxylase, both stabilizations and destabilization were detected (see discussion above).

Added Proteomic Coverage

The iTRAQ-SPROX experiments in this work enabled 128 yeast proteins that were not previously assayed in SILAC-SPROX to be assayed for AMP-PNP-interactions. The iTRAQ-SPROX experiments also enabled some proteins previously assayed in SILAC-SPROX to be assayed with additional methionine-containing peptide probes. In total, the iTRAQ-SPROX experiment led to the detection of 11 additional ATP-sensitive proteins, including five that were not previously annotated as ATP-binding proteins in the SGD (see Table 2). Also, among the 28 protein hits identified in the iTRAQ-SPROX experiment were a group of four previously annotated ATP-binding proteins that were not identified as hits in the SILAC-SPROX experiments, even though all four of these previously annotated ATP binding proteins were assayed in the SILAC-SPROX experiments (see Table 2). Given that these proteins are annotated ATP-binding proteins, it is likely that these four proteins were false negatives in the SILAC-SPROX experiments. In one case, the peptide identification was missing at a critical denaturant concentration in the SILAC-SPROX experiment, in another case the L/H ratios of the peptide barely missed (i.e., were within 10% of) the hit selection criteria, and in the other two cases it is unclear why the proteins were false negatives in the SILAC-SPROX experiment.

Table 3. Summary of Protein Classes Represented by the 150 ATP-Binding Protein Hits Identified in the iTRAQ-SPROX Experiments in This Work and in the SILAC-SPROX Experiments Described in Reference [35]. Also Summarized are the Protein Classes Represented by All the 668 Proteins Annotated with the GO Term "ATP-binding" in the *Saccharomyces* Genome Database

Protein class	44 Annotated hits (%)	106 Novel hits (%)	All 668 annotated yeast proteins (%)
Transferase	8.3	7.0	21.5
Chaperone	16.7	2.0	4.0
Ligase	20.0	1.0	10.0
Nucleic acid binding	13.3	39.0	17.5
Hydrolase	11.7	10.0	10.7
Kinase	6.7	1.0	19.1
Transporter	10.0	1.0	5.5
Oxidoreductase	1.7	13.0	1.1
Other	11.8 [a]	22.0 [b]	10.6 [c]

[a]Includes five additional protein classes each containing ≤5% of the previously annotated hits
[b]Includes 10 additional protein classes each containing <10% of the novel hits
[c]Includes 13 additional protein classes each containing <3% of all annotated yeast proteins

Discovery of Novel ATP-Interacting Proteins

The ATP-sensitive protein hits identified in the iTRAQ-SPROX experiments described here included 14 proteins that were not previously annotated as ATP-binding proteins in the SGD (Table 2). Included in this set of 14 proteins was a subset of nine proteins that were also identified as ATP-interacting protein hits using the SILAC-SPROX technique [35]. Together, the iTRAQ-SPROX and SILAC-SPROX techniques identified a total of 150 ATP-sensitive proteins including 106 proteins that were not previously annotated as ATP-binding proteins in the SGD (see Supplementary Table S2).

A bioinformatics analysis using PANTHER [45] to characterize these 106 newly discovered ATP-interacting proteins revealed that the largest fractions of these proteins were nucleic acid-binding proteins, hydrolases, oxidoreductases, and transferases (Table 3). The set of 106 newly discovered ATP-sensitive proteins did not contain significant numbers of kinases, ligases, or chaperones. The proteins in each of these classes constituted <5% of the newly discovered ATP-interacting proteins. In contrast, kinases, ligases, and chaperones, which are all well known to have ATP-binding activity, were well-represented in the 44 annotated ATP-binding protein hits and in all the yeast proteins that are currently annotated as ATP-binding proteins in the SGD (Table 3).

The well-known ATP-binding properties of kinases, ligases, and chaperones enabled an estimation of the false negative rates associated with the iTRAQ- and SILAC-SPROX experiments. The 660 assayed proteins in the iTRAQ- and SILAC-SPROX experiments included 38 ligases, 31 chaperones, and 15 kinases. Approximately 30%–40% of the proteins in each of these protein classes were successfully detected as hits. The remaining 60%–70% of the ligases, chaperones, and kinases may not have been detected because the ligand-induced stability changes were not large enough to be measured by the iTRAQ- and SILAC-SPROX techniques. For example, binding interactions with K_d values >2 mM would not have been detected in these experiments because they would not have

produced transition midpoint shifts greater than or equal to 1 M, which was the minimum shift deemed significant in these studies (see iTRAQ Data Analysis section in Experimental). It is also possible that some proteins do not have properly positioned methionine residues in their three-dimensional structures to successfully report on AMP-PNP binding.

The relatively low representation of kinases, ligases, and chaperones in the novel hits suggests that the bioinformatics approaches used to identify ATP-binding proteins work well for protein kinases, ligases, and chaperones. For example, many protein kinases contain the phosphate loop (P-loop) binding motif [46], which is a known binding site for ATP and GTP that is amenable to detection using bioinformatics approaches. However, not all ATP-binding proteins contain P-loop motifs or other well-characterized ATP-binding pockets [46]. Significant percentages (>10%) of the novel hits detected in this study were nucleic acid-binding proteins, hydrolases, and oxidoreductases (Table 3). This suggests that the ATP-interaction properties of proteins in these classes are less well-predicted using existing bioinformatics approaches. This underscores the need for experimental approaches, such as the iTRAQ-SPROX technique used here, to better understand protein-ATP interactions.

Conclusion

The iTRAQ-SPROX methodology was used here to identify ATP-sensitive proteins in the *Saccharomyces cerevisiae* proteome. A total of 28 ATP-sensitive protein hits were identified, and half of the identified proteins were previously annotated as ATP-binding proteins in the SGD database. The other half of the protein hits identified here included nine proteins that were also found to be sensitive to ATP-induced thermodynamic stability changes using the SILAC-SPROX technique [35]. Together, the iTRAQ-SPROX experiments described here and the SILAC-SPROX experiments described in reference [35] facilitated the analysis of 660 yeast proteins for ATP interactions. While the proteomic coverage observed in the SILAC-SPROX experiments (532 proteins) was greater than that in the iTRAQ-SPROX experiments described here (373 proteins), there was a subset of 128 proteins that were exclusively assayed by iTRAQ-SPROX. In total, 150 ATP-sensitive proteins were identified using the iTRAQ- and SILAC-SPROX techniques. Among these ATP-sensitive proteins were a group of 44 previously annotated ATP-binding proteins that included many kinases, ligases, and chaperones. The 106 newly discovered ATP-sensitive proteins included many hydrolases, oxidoreductases, and nucleic acid binding proteins.

Acknowledgments

The authors thank the Proteomics Facility at the Fred Hutchinson Cancer Research Center for collecting the LC-MS/MS data in Experiment 1. They also thank the Duke Proteomics Facility, specifically Laura Dubois, for collecting the LC-MS/MS data in Experiment 2.
This work was supported by a grant from the National Science Foundation (CHE-1308093) to M.C.F.

References

1. Alder, N.N., Theg, S.M.: Energy use by biological protein transport pathways. Trends Biochem. Sci. **28**, 442–451 (2003)
2. Buttgereit, F., Brand, M.D.: A hierarchy of ATP-consuming processes in mammalian-cells. Biochem. J. **312**, 163–167 (1995)
3. Clare, D.K., Saibil, H.R.: ATP-driven molecular chaperone machines. Biopolymers **99**, 846–859 (2013)
4. Fawaz, M.V., Topper, M.E., Firestine, S.M.: The ATP-grasp enzymes. Bioorg. Chem. **39**, 185–191 (2011)
5. Palfrey, H.C., Pewitt, E.B.: The ATP and Mg2+ dependence of Na+-K+-2cl- cotransport reflects a requirement for protein-phosphorylation - studies using calyculin-A. Pflug Arch. Eur. J. Phys **425**, 321–328 (1993)
6. Ali, M.M., Roe, S.M., Vaughan, C.K., Meyer, P., Panaretou, B., Piper, P.W., Prodromou, C., Pearl, L.H.: Crystal structure of an Hsp90-nucleotide-p23/Sba1 closed chaperone complex. Nature **440**, 1013–1017 (2006)
7. Balbo, P.B., Bohm, A.: Mechanism of poly(A) polymerase: structure of the enzyme-MgATP-RNA ternary complex and kinetic analysis. Structure **15**, 1117–1131 (2007)
8. Cavarelli, J., Eriani, G., Rees, B., Ruff, M., Boeglin, M., Mitschler, A., Martin, F., Gangloff, J., Thierry, J. C., Moras, D.: The active site of yeast aspartyl-tRNA synthetase: structural and functional aspects of the aminoacylation reaction. EMBO J. **13**, 327–337 (1994)
9. Dautant, A., Velours, J., Giraud, M.F.: Crystal structure of the Mg.ADP-inhibited state of the yeast F1c10-ATP synthase. J. Biol. Chem. **285**, 29502–29510 (2010)
10. Dupin, A.E., Fribourg, S.: Structural basis for ATP loss by C1p1p in a G135R mutant protein. Biochimie **101C**, 203–207 (2014)
11. Fenn, S., Breitsprecher, D., Gerhold, C.B., Witte, G., Faix, J., Hopfner, K.P.: Structural biochemistry of nuclear actin-related proteins 4 and 8 reveals their interaction with actin. EMBO J. **30**, 2153–2166 (2011)
12. Liu, Q., Hendrickson, W.A.: Insights into Hsp70 chaperone activity from a crystal structure of the yeast Hsp110 Sse1. Cell **131**, 106–120 (2007)
13. Liu, X., Bushnell, D.A., Silva, D.A., Huang, X., Kornberg, R.D.: Initiation complex structure and promoter proofreading. Science **333**, 633–637 (2011)
14. Noble, C.G., Beuth, B., Taylor, I.A.: Structure of a nucleotide-bound Clp1-Pcf11 polyadenylation factor. Nucleic Acids Res. **35**, 87–99 (2007)
15. Nolen, B., Ngo, J., Chakrabarti, S., Vu, D., Adams, J.A., Ghosh, G.: Nucleotide-induced conformational changes in the Saccharomyces cerevisiae SR protein kinase, Sky1p, revealed by X-ray crystallography. Biochemistry **42**, 9575–9585 (2003)
16. Otomo, T., Tomchick, D.R., Otomo, C., Panchal, S.C., Machius, M., Rosen, M.K.: Structural basis of actin filament nucleation and processive capping by a formin homology 2 domain. Nature **433**, 488–494 (2005)
17. Padyana, A.K., Qiu, H., Roll-Mecak, A., Hinnebusch, A.G., Burley, S.K.: Structural basis for autoinhibition and mutational activation of eukaryotic initiation factor 2alpha protein kinase GCN2. J. Biol. Chem. **280**, 29289–29299 (2005)
18. Polier, S., Dragovic, Z., Hartl, F.U., Bracher, A.: Structural basis for the cooperation of Hsp70 and Hsp110 chaperones in protein folding. Cell **133**, 1068–1079 (2008)
19. Robinson, G.C., Bason, J.V., Montgomery, M.G., Fearnley, I.M., Mueller, D.M., Leslie, A.G., Walker, J.E.: The structure of F(1)-ATPase from Saccharomyces cerevisiae inhibited by its regulatory protein IF(1). Open Biology **3**, 120164 (2013)
20. Schmidt, H., Gleave, E.S., Carter, A.P.: Insights into dynein motor domain function from a 3.3-A crystal structure. Nat. Struct. Mol. Biol. **19**, 492–497, S491 (2012)
21. Ugochukwu, E., Lovering, A.L., Mather, O.C., Young, T.W., White, S.A.: The crystal structure of the cytosolic exopolyphosphatase from *Saccharomyces cerevisiae* reveals the basis for substrate specificity. J. Mol. Biol. **371**, 1007–1021 (2007)
22. Vorobiev, S., Strokopytov, B., Drubin, D.G., Frieden, C., Ono, S., Condeelis, J., Rubenstein, P. A., Almo, S. C.: The structure of nonvertebrate actin: implications for the ATP hydrolytic mechanism. Proc. Natl. Adad. Sci U.S.A. **100**, 5760–5765 (2003)

23. Watson, H.C., Walker, N.P., Shaw, P.J., Bryant, T.N., Wendell, P.L., Fothergill, L.A., Perkins, R.E., Conroy, S.C., Dobson, M.J., Tuite, M.F., Kinsgman, A.J., Kingsman, S.M.: Sequence and structure of yeast phosphoglycerate kinase. EMBO J. **1**, 1635–1640 (1982)
24. Westover, K.D., Bushnell, D.A., Kornberg, R.D.: Structural basis of transcription: nucleotide selection by rotation in the RNA polymerase II active center. Cell **119**, 481–489 (2004)
25. Kubala, M.: ATP-binding to P-type ATPases as revealed by biochemical, spectroscopic, and crystallographic experiments. Proteins **64**, 1–12 (2006)
26. McAllister, F.E., Niepel, M., Haas, W., Huttlin, E., Sorger, P.K., Gygi, S.P.: Mass spectrometry based method to increase throughput for kinome analyses using ATP probes. Anal. Chem. **85**, 4666–4674 (2013)
27. Wolfe, L.M., Veeraraghavan, U., Idicula-Thomas, S., Schurer, S., Wennerberg, K., Reynolds, R., Besra, G.S., Dobos, K.M.: A chemical proteomics approach to profiling the ATP-binding proteome of Mycobacterium tuberculosis. Mol. Cell Proteomics **12**, 1644–1660 (2013)
28. Patricelli, M.P., Szardenings, A.K., Liyanage, M., Nomanbhoy, T.K., Wu, M., Weissig, H., et al.: Functional interrogation of the kinome using nucleotide acyl phosphates. Biochemistry **46**, 350–358 (2007)
29. Patricelli, M.P., Nomanbhoy, T.K., Wu, J., Brown, H., Zhou, D., Zhang, J., Jagannathan, S., Aban, A., Okerberg, E., Herring, C., Nordin, B., Weissig, H., Yang, Q., Lee, J.D., Gray, N.S., Kozarich, J.W..: In situ kinase profiling reveals functionally relevant properties of native kinases. Chem. Biol. **18**, 699–710 (2011)
30. Adachi, J., Kishida, M., Watanabe, S., Hashimoto, Y., Fukamizu, K., Tomonaga, T.: Proteome-wide discovery of unknown ATP-binding proteins and kinase inhibitor target proteins using an ATP probe. J. Prot. Res. **13**, 5461–5470 (2014)
31. Xiao, Y., Guo, L., Jiang, X., Wang, Y.: Proteome-wide discovery and characterizations of nucleotide-binding proteins with affinity-labeled chemical probes. Anal. Chem. **85**, 3198–3206 (2013)
32. Xiao, Y., Guo, L., Wang, Y.: Isotope-coded ATP probe for quantitative affinity profiling of ATP-binding proteins. Anal. Chem. **85**, 7478–7486 (2013)
33. Liu, P.F., Kihara, D., Park, C.: Energetics-based discovery of protein-ligand interactions on a proteomic scale. J. Mol. Biol. **408**, 147–162 (2011)
34. Chang, Y., Schlebach, J.P., VerHeul, R.A., Park, C.: Simplified proteomics approach to discover protein-ligand interactions. Protein Sci. **21**, 1280–1287 (2012)
35. Tran, D.T., Adhikari, J., Fitzgerald, M.C.: Stable isotope labeling with amino acids in cell culture (SILAC)-based strategy for proteome-wide thermodynamic analysis of protein-ligand binding interactions. Mol. Cell. Proteomics **13**, 1800–1813 (2014)
36. Savitski, M.M., Reinhard, F.B., Franken, H., Werner, T., Savitski, M.F., Eberhard, D., Molina, D.M, Jafari, R., Dovega, R.B., Klaeger, S., Kuster, B., Nordlund, P., Bantscheff, M., Drewes, G.: Tracking cancer drugs in living cells by thermal profiling of the proteome. Science **346**, 1255784 (2014)
37. Strickland, E.C., Geer, M.A., Tran, D.T., Adhikari, J., West, G.M., DeArmond, P.D., Xu, Y., Fitzgerald, M.C.: Thermodynamic analysis of protein-ligand binding interactions in complex biological mixtures using the stability of proteins from rates of oxidation. Nat. Protoc. **8**, 148–161 (2013)
38. Myers, J.K., Pace, C.N., Scholtz, J.M.: Denaturant m values and heat capacity changes: relation to changes in accessible surface areas of protein unfolding. Protein Sci. **4**, 2138–2148 (1995)
39. Szklarczyk, D., Franceschini, A., Wyder, S., Forslund, K., Heller, D., Huerta-Cepas, J., Simonovic, M., Roth, A., Santos, A., Tsafou, K.P., Kuhn, M., Bork, P., Jensen, L.J., von Mering, C.: STRING v10: protein-protein interaction networks, integrated over the tree of life. Nucleic Acids Res. **43**, D447–D452 (2015)
40. West, G.M., Tang, L., Fitzgerald, M.C.: Thermodynamic analysis of protein stability and ligand binding using a chemical modification- and mass spectrometry-based strategy. Anal. Chem. **80**, 4175–4185 (2008)
41. Ng, S.K., Hamilton, I.R.: Purification and regulatory properties of pyruvate kinase from Veillonella parvula. J. Bacteriol. **122**, 1274–1282 (1975)
42. Seidler, N.W.: Dynamic oligomeric properties. Adv. Exp. Med. Biol. **985**, 207–247 (2013)
43. Liu, P.F., Park, C.: Selective stabilization of a partially unfolded protein by a metabolite. J. Mol. Biol. **422**, 403–413 (2012)
44. Gierasch, L.M.: Caught in the act: how ATP binding triggers cooperative conformational changes in a molecular machine. Mol. Cell **9**, 3–5 (2002)
45. Mi, H.Y., Muruganujan, A., Casagrande, J.T., Thomas, P.D.: Large-scale gene function analysis with the PANTHER classification system. Nat. Protoc. **8**, 1551–1566 (2013)
46. Saraste, M., Sibbald, P.R., Wittinghofer, A.: The P-loop—a common motif in ATP-binding and GTP-binding proteins. Trends Biochem. Sci. **15**, 430–434 (1990)